VTT Technical Research Centre of Finland

Simulation of incompressible viscous flow around a ducted propeller using a RANS equation solver

Sanchez Caja, Antonio; Rautaheimo, Patrik; Siikonen, Timo

Published in:
Proceedings of the 23rd Symposium on Naval Hydrodynamics

Published: 01/01/2001

Document Version
Publisher's final version

Simulation of Incompressible Viscous Flow Around a Ducted Propeller Using a RANS Equation Solver

A. Sánchez-Caja,
(VTT Manufacturing Technology, Finland)
P. Rautaheimo and T. Siikonen
(Helsinki University of Technology, Finland)

ABSTRACT

The incompressible viscous flow around a marine ducted propeller is simulated by solving the RANS equations with the k-ε turbulence model. The FINFLO solver developed at Helsinki University of Technology is used in the calculations. FINFLO is a multiblock cell-centered finite-volume computer code with sliding mesh, moving-grid and free-surface capabilities. In this paper, the flow over a Ka series propeller and NSMB nozzle 19A is analyzed. The calculated flow patterns downstream of the propeller and duct are illustrated and compared with experiments for one advance number. Calculated thrust and torque are also provided for several advance numbers. Good correlation with experiments is obtained in terms of force coefficients and velocity distributions.

INTRODUCTION

Ducted propulsors are known to offer significant advantages for particular marine applications. Since 1931, they have been first installed in tugs, push-boats, trawlers, and later in research vessels, drilling platforms, submersibles, etc. There are some installations in commercial ships, like large tankers and bulk carriers, and warships like naval destroyers and submarines. Among the benefits of ducted propulsors are remarkable increases in efficiency for high propeller loadings with flow-accelerating ducts, or alternatively smaller propeller size; reduction of inflow velocity and, consequently, of cavitation and noise with flow-decelerating ducts; better control over the inflow to the propeller; improvement of maneuverability and position-keeping abilities of vessels; protection from damage to the propeller, etc.

From a theoretical standpoint, the hydrodynamic interaction between duct and propeller produces a twofold effect. On the one hand, the presence of the duct permits to transfer the mean lifting force on the propeller blade closer to the propeller tip, which in turn efficiently deflects the force to a direction near that of the ship's motion. On the other hand, the radial contraction of the flow due to the propeller action results in an additional thrusting force on the duct, which increases the total thrust of the propulsor unit provided that the loading is sufficiently high to overcome the duct viscous drag. However, there is an upper limit also for the duct loading, which is determined by the risk of flow separation, as well as for the propeller loading, which is determined by the risk of cavitation at the propeller tip. The design of a ducted propeller is, therefore, a complicated process in which the designer often has to make a compromise between conflicting requirements. In such cases, having access to information on the details of the flowfield in problematic areas is most valuable for a successful design.

Most of the analysis methods for ducted propulsors have been based on potential theory, using an actuator disk (Gibson and Lewis, 1973; Gibson, 1974; Falcão de Campos, 1983, etc.), lifting-line or lifting-surface approaches (Kerwin et al. 1987; Hughes & Kinnas, 1991, etc.) for modeling the propeller. The more recent panel methods also belong

to this class of potential-based theories (Hoshino 1989, Kawakita 1992, etc.). All these methods represent a great advance in understanding the main features of the flow around ducted propulsors. However, they all have the shortcoming of incorporating viscous effects artificially through empirical corrections external to the theory. In other words, details as important to the designer as the gap flow at the tip of the propeller cannot be properly analyzed with these methods. Recently, some hybrid models have been developed that combine viscous and potential theories mainly for the design problem, for example, in Kerwin et al. (1994). More recently, calculations of the flow around a ducted thruster have been made at Postdam Model Basin for Schottel Shipyard GmbH using either hybrid or fully viscous models. This work has been outlined in Abdel-Maksoud (1999), but no validation data were released. In the present paper, the RANS equations are solved for a ducted propeller configuration using the FINFLO code initially developed at the Laboratory of Aerodynamics at Helsinki University of Technology (Siikonen, 1990). The flow around a ducted propeller of the NSMB (now MARIN) Ka series is simulated and compared to experimental data from the cavitation tunnel of the Nagasaki Experimental Tank (Kawakita, 1992). The experimental data reported by Kawakita are among the few available in the open literature for the validation of ducted propellers.

FINFLO is a multiblock cell-centered finite-volume multigrid-structured computer code with sliding mesh, moving-grid and free-surface capabilities. The code has been validated for a number of test cases including marine applications. For propeller flows, validation work was carried out for conventional propeller geometries such as that of DTMB propeller 4119 (Sánchez-Caja, 1998). Recently, the unsteady flow around a tractor thruster was simulated using a sliding mesh technique and a comparison of some available experimental data to computed results was presented (Sánchez-Caja, et al. 1999). The sliding mesh technique was found robust for the analysis of the time-dependent viscous flow. The computations were performed in a quasi-steady and time-accurate manner. The former reduced the CPU time to about 1/10 relative to the latter. Its main merit consisted of decreasing the CPU time while maintaining a full representation of the propeller geometry, i.e. without introducing simplified models for simulating the propeller action, such as actuator disk or body force models.

In the present study, the flow around a ducted propeller unit is considered. Even though the unit consists of a rotating part (the propeller) and a stationary part (the duct), a steady-state flow can be assumed provided that the inflow and duct are axisymmetric. Consequently, there is no need to use special techniques based on overlapping or sliding meshes.

NUMERICAL METHOD

Governing Equations and Turbulence Closure

The flow simulation is based on the solution of the RANS equations. These can be written in the following conservative form

$$\frac{\partial U}{\partial t}+\frac{\partial (F-F_v)}{\partial x}+\frac{\partial (G-G_v)}{\partial y}+\frac{\partial (H-H_v)}{\partial z}=Q \quad (1)$$

where U is a vector of conservative variables (ρ, ρu, ρv, ρw, ρk, $\rho \varepsilon$)$^{\mathrm{T}}$; F, G and H are the inviscid fluxes; F_v, G_v and H_v are the viscous fluxes; u, v and w are the absolute velocity components; ρ is the density, k is the turbulent kinetic energy and ε is the dissipation of k. The source term Q has non-zero components only for the turbulence equations. For the steady-state propeller analysis, the equations are solved in a co-ordinate system that rotates around the x-axis with an angular velocity Ω. In this case, Q has the additional component (0, 0, $\rho\Omega w$, $-\rho\Omega v$, 0, 0). For time-accurate simulations, the source terms for the turbulence equations are retained, but there are no source terms in the momentum equations.

In the low-Reynolds number k-ε model, the solution is extended to the wall instead of using a wall-function approach (Chien, 1982). The source term for Chien's model is given as

$$Q=\begin{pmatrix} P-\rho\tilde{\varepsilon}-2\mu\dfrac{k}{y_n^2} \\ c_1\dfrac{\tilde{\varepsilon}}{k}P-c_2\dfrac{\rho\tilde{\varepsilon}^2}{k}-2\mu\dfrac{\tilde{\varepsilon}}{y_n^2}e^{-y^+/2} \end{pmatrix} \quad (2)$$

In Chien's model $\tilde{\varepsilon}$ is solved instead of ε. The variable $\tilde{\varepsilon}$ is defined so that it obtains a zero value at

the wall and the true dissipation can be expressed as $\varepsilon = \tilde{\varepsilon} + 2\frac{\mu}{\rho}\frac{k}{y_n^2}$.

The equations for k and ε contain empirical coefficients. In this study, the following coefficients are applied,

$$\begin{aligned} c_1 &= 1.44 \\ c_2 &= 1.92(1-0.22e^{-\mathrm{Re}_T^2/36}) \\ c_\mu &= 0.09(1-e^{-0.0115y^+}) \end{aligned} \qquad \begin{aligned} \sigma_k &= 1.0 \\ \sigma_\varepsilon &= 1.3 \end{aligned} \tag{3}$$

where the turbulence Reynolds number is defined as

$$\mathrm{Re}_T = \frac{\rho k^2}{\mu\tilde{\varepsilon}}$$

Pseudo-compressibility

The FINFLO RANS solver utilizes a structured multiblock grid. The code was initially developed for compressible flows (Siikonen, 1990) and it has been extended to incompressible flows using a pseudo-compressibility method (Chorin, 1967). In the pseudo-compressibility approach the continuity equation $\nabla \cdot \vec{V} = 0$ is replaced by

$$\frac{1}{\beta^2}\frac{\partial p}{\partial t} + \nabla \cdot \vec{V} = 0 \tag{4}$$

In the actual implementation of the present method, all the derivatives $\partial\rho/\partial p$ are replaced by a pseudo-compressibility factor β^2 (Rahman et al., 1997). In this way, the characteristic speeds reduce to simple expressions of $\lambda_{1,2} = u \pm \beta$. The flux calculation is based on a simplification of Roe's method (Roe, 1981). The implicit stage uses an approximate factorization and a multigrid method is applied for the acceleration of convergence.

Discretization

A finite-volume technique is used for solving the equations. The differential equations are integrated over a computational cell

$$V_i \frac{dU_i}{dt} = \sum_{faces} -SF^* + V_i Q_i \tag{5}$$

where

$$F^* = n_x(F - F_v) + n_y(G - G_v) + n_z(H - H_v) \tag{6}$$

and the summation is extended over the faces of the computational cell. In a rotating frame, i.e. for propeller calculations, the functional form of the flux equations is similar to the case without rotation. The difference is that in a rotating frame the motion of the cell faces is taken into account in the evaluation of convective velocities (Siikonen and Pan, 1992).

The inviscid flux is calculated with the help of a rotation matrix, which transforms the dependent variables to a local system of coordinates normal to the cell surface (Siikonen, 1994). The interface values are evaluated by a MUSCL-type formula.

Solution Algorithm

For steady-state flow simulations, the discretized equations are integrated in time by applying the DDADI factorization (Lombard et al. 1983). This is based on splitting the Jacobians of the flux terms. The resulting approximately factored implicit scheme consists of a backward and a forward sweep in every coordinate direction. The sweeps are based on first-order upwind differencing. In order to accelerate convergence, local time-stepping and a multigrid method are also implemented in FINFLO (Siikonen et al., 1990). In time-accurate simulations for unsteady flows, the above-mentioned pseudo-time integration is performed inside a physical time-step (Sánchez et al., 1999). More detailed descriptions of FINFLO can be found in Siikonen et al. (1990), Siikonen & Pan (1992) and Pitkänen & Siikonen (1995).

NUMERICAL RESULTS

Geometry, Mesh and Boundary Conditions

The case selected for analysis is the ducted propeller presented in Kawakita (1992). The propeller has five blades, a diameter of 0.221 m and a pitch ratio of 0.9741. It belongs to the NSMB Ka series. The duct is NSMB nozzle no. 19A. The clearance at the propeller tip is 0.72% of the propeller diameter. LDV measurements were reported at a rate of rotation of 25 rps corresponding to an advance coefficient of

0.5. The thrust and torque were measured as well as the velocities downstream of the propeller. Computations were performed under the same conditions. Two additional computations were performed for advance coefficients of 0.35 and 0.65. The axial inflow was varied keeping the propeller rotational speed constant, as in the tests. Only thrust and torque measurements were available for comparison for these last computations.

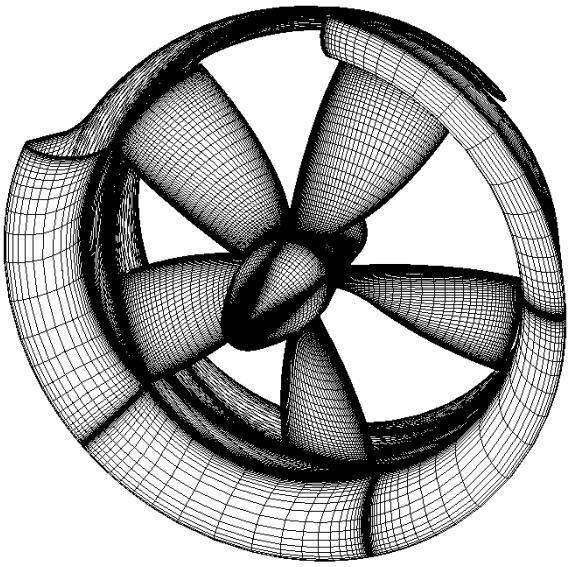

Figure 1. Grid on the surface of the ducted propeller. Detail of grid construction on the duct.

The grid used in the computations has over one million cells, as shown in Table I. Special emphasis was put on modeling the propeller blades and their near-wakes accurately. The only noticeable difference in geometry from the ducted propeller model was that the hub of the computational grid was extended downstream of the propeller, as is the practice of MARIN, whereas the experimental model has it extended upstream. Only the portion between two contiguous blades has been used in the computations due to the periodicity of the solution. Figure 1 illustrates the grid shape on the duct and propeller surfaces, and Figure 2 shows the topology.

Table I. Number of cells in the mesh

Propeller	Duct	Rest	Total Grid
562,688	154,112	440,832	1,157,632

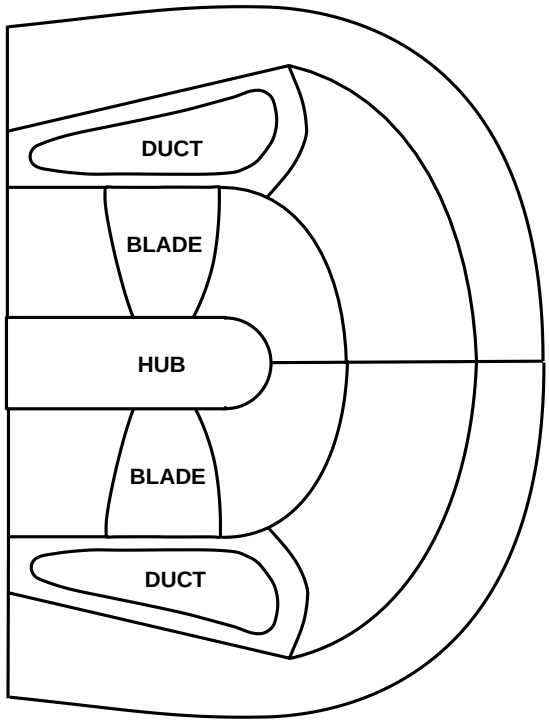

Figure 2. Grid topology.

The topology was H-type around the propeller blades with over a half-million cells inside the duct, and O-type around the duct. The grid has the inlet boundary modeled by a spherical sector located at more than three diameters from the propeller center. The outlet boundary is a plane located at an axial location between 3 and 4 propeller diameters from the propeller center. Fine grid spacings are used in the vicinity of the leading and trailing edges of the propeller blades in the chordwise direction, and near the blade and tip in the radial direction. The minimum grid spacing in the circumferential direction for the resolution of the boundary layer was such that the y+ parameter was found to be about 1-1.5 over most of the blade, and 1 on the duct surface. A total of 19 blocks was used in order to distribute the computing load between 8 processors.

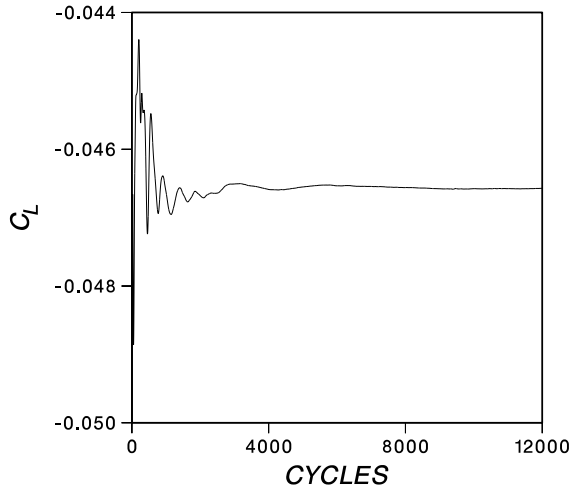

Figure 3. Convergence history of the overall lift coefficient.

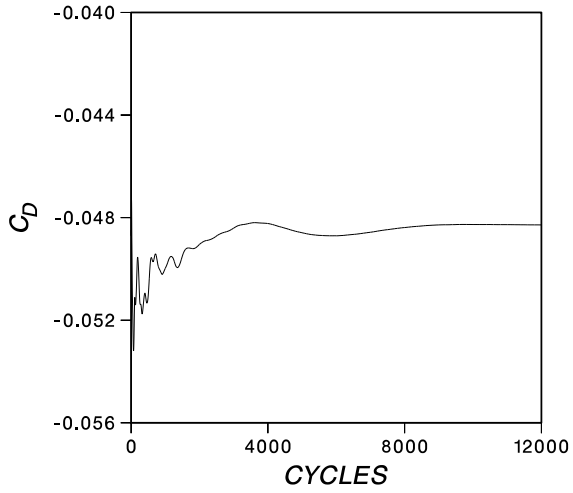

Figure 4. Convergence history of the overall drag coefficient.

The hub and blade surfaces of the propeller are rotating solid walls with boundary conditions enforcing the velocity field to match the propeller rotational speed. The velocities at the duct surface are set to zero in order to satisfy the non-slip boundary condition. The lateral surfaces adjacent to the propeller blades and duct have cyclic or periodic boundary conditions. The block boundaries where two adjacent block surfaces are coincident are defined as connectivities. A uniform flow condition is applied to the inlet and peripherical surfaces. The streamwise gradients of the flow variables are set to zero at the outlet.

Convergence

The computations were performed on an SGI Origin 2000 machine. Eight processors were used. The computation time was 13 seconds per iteration cycle. For the second grid level, the computation time was 1/8 times that of the first grid level. A satisfactory convergence was obtained with a Courant number of 0.5 using two multigrid levels.

The convergence histories of the overall lift and drag coefficients are presented in Figs. 3 and 4. After 3000 iterations, the overall drag coefficient converged within 1% of the final value, and the overall lift coefficient within 0.5%. Figure 5 shows a magnification of the convergence history for the overall lift coefficient.

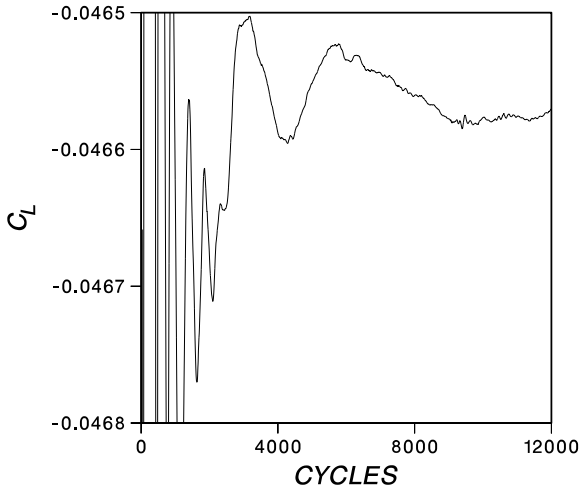

Figure 5. Convergence history of the overall lift coefficient. Magnification.

Forces and Pressures

The k-ε turbulence model gave a good correlation of flow patterns and performance coefficients with measurements. Table II shows that the performance coefficients were calculated for advance number 0.5 within 4.5% of the measurements. In particular, the thrust coefficient for the propeller (K_{TP}) was predicted very accurately. The difference of about 4% from measurements in the prediction of duct thrust (K_{TD})

made a total difference in the total thrust coefficient (K_T) of less than 1%. The torque coefficient (K_Q) was overpredicted by about 4.5%. For other advance numbers, the differences in thrust were a little higher but reasonable, although the torque was better predicted. Figure 6 compares the experimental performance coefficients to the calculations for three advance numbers.

Table II. Experimental and calculated performance coefficients for J=0.5

	Experiment (*)	Calculations	
		1st level	2nd level
K_{TP}	0.197	0.197	0.220
K_{TD}	0.048	0.046	0.042
K_T	0.245	0.243	0.263
K_Q	0.0345	0.0361	0.0418

(*) as read from the test diagram in Kawakita (1992)

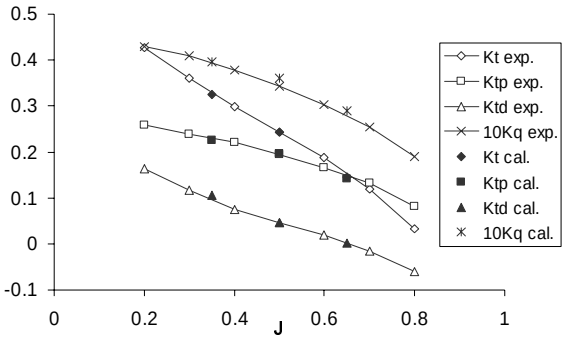

Figure 6. Comparison of experimental and calculated thrust and torque coefficients for several advance numbers.

The calculated pressure distribution on the ducted propeller surfaces is shown for the suction and the pressure side of the propeller blades in Figures 7 and 8, respectively. A low-pressure area can be identified in Figure 7 at the suction side of the propeller tip extending to the duct surface.

Figure 8 shows a large area of moderate negative pressures at the pressure side of the propeller blades. The duct accelerates the inflow to the propeller, which results in a large extent of low pressures on the propeller blades compared with a corresponding open propeller.

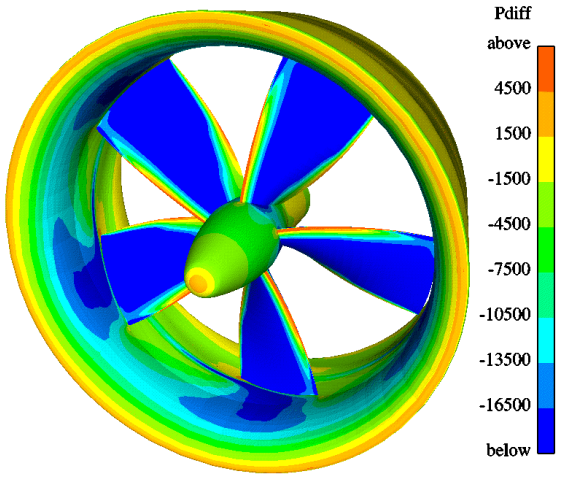

Figure 7. Distribution of pressure difference on the suction side of ducted propeller NSMB 19A.

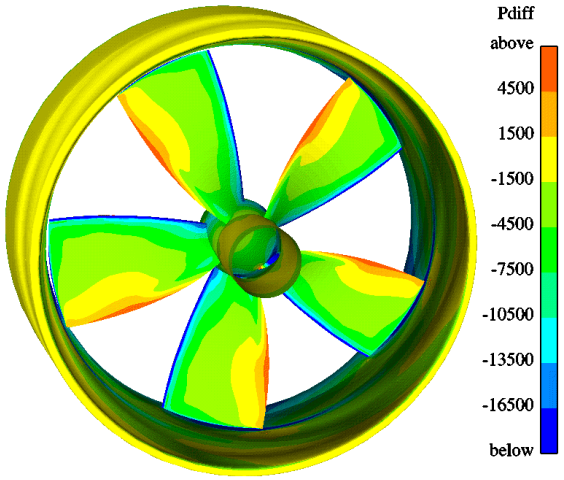

Figure 8. Distribution of pressure difference on the pressure side of ducted propeller NSMB 19A.

Velocities and Hydrodynamic Pitch

Figure 9 illustrates the circumferential variations of the velocity components downstream of the propeller plane at r/R=0.5, 0.9, 1.0 and 1.05, and at x/R=0.65 (just behind the duct) for both experiments and calculations. The velocities are non-dimensionalized with the axial inflow. The advance number is 0.5. Each velocity fluctuates with the blade frequency. The computations show the same trends as the experiments reported in Figure 3 by Kawakita (1992).

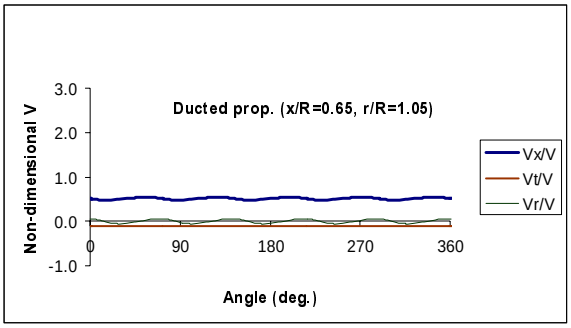

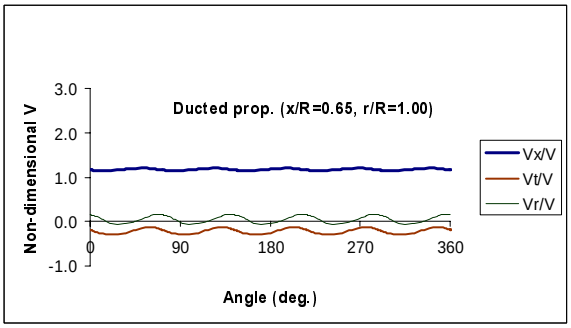

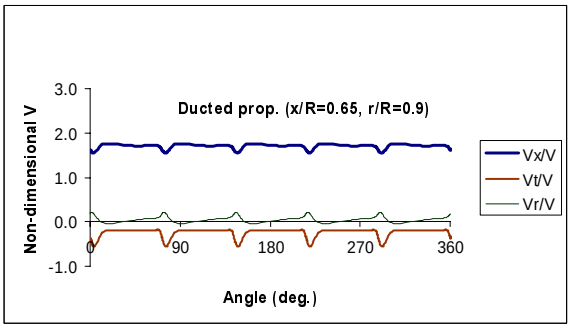

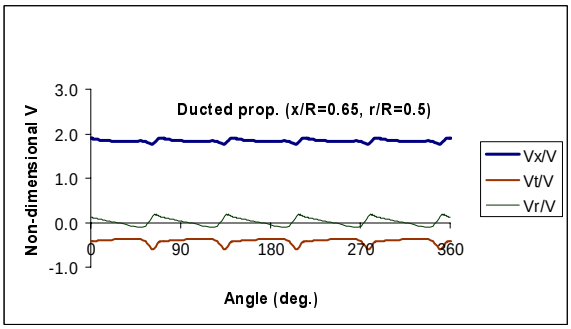

Figure 9 Calculated circumferential variations of velocity components downstream of the propeller at x/R=0.65 and r/R=0.5, 0.9, 1.0, and 1.05.

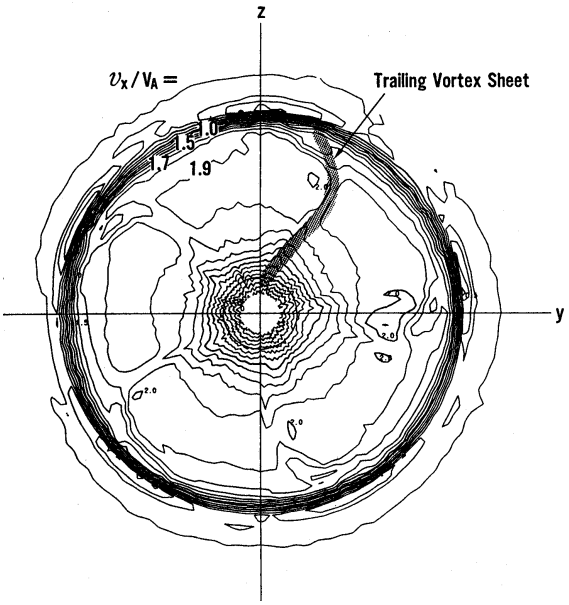

Figure 10a. Velocity contours downstream of the ducted propeller (J=0.50, x/R=0.65). (Kawakita, 1992).

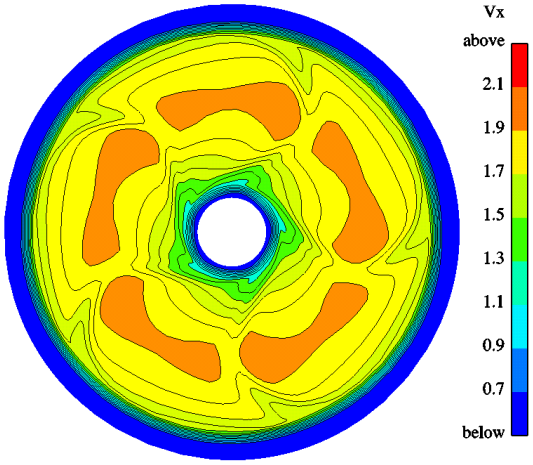

Figure 10b. Calculated velocity contours downstream of the ducted propeller (J=0.50, x/R=0.65).

Figures 10a and 10b provide a comparison of experimental and calculated velocity contours at the same axial location. The location and shape of the calculated trailing vortex sheet is apparent from the figures and coincides with that of the experiments. The agreement is good. Figures 11a and 11b compare the experimental and calculated velocity vectors,

respectively. The agreement is good except for the fact that the grid is not completely aligned with the propeller trailing wake, which results in some lack of circumferential grid resolution and consequently in a prediction of tip vortex weaker than in the experiments.

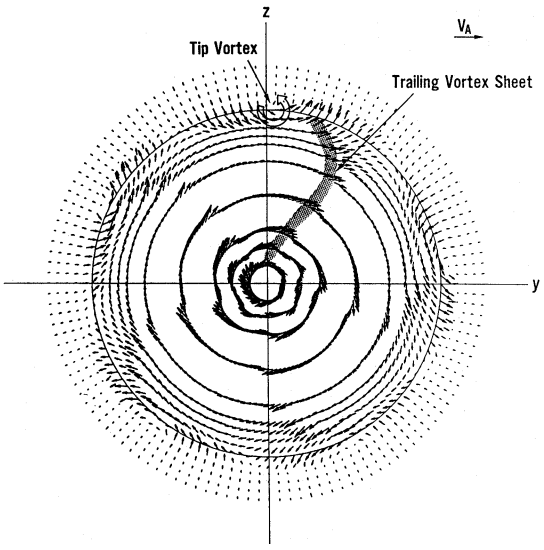

Figure 11a. Tangential and radial velocity field downstream of the ducted propeller (J=0.50, x/R=0.65). (Kawakita, 1992).

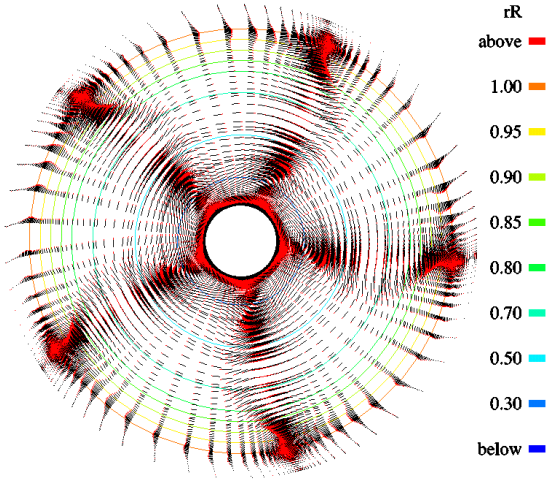

Figure 11b. Calculated tangential and radial velocity field downstream of the ducted propeller (J=0.50, x/R=0.65).

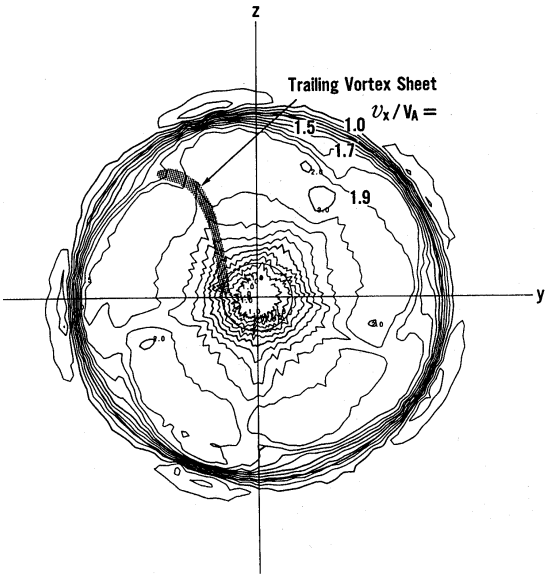

Figure 12a. Velocity contours downstream of the ducted propeller (J=0.50, x/R=1.00). (Kawakita, 1992).

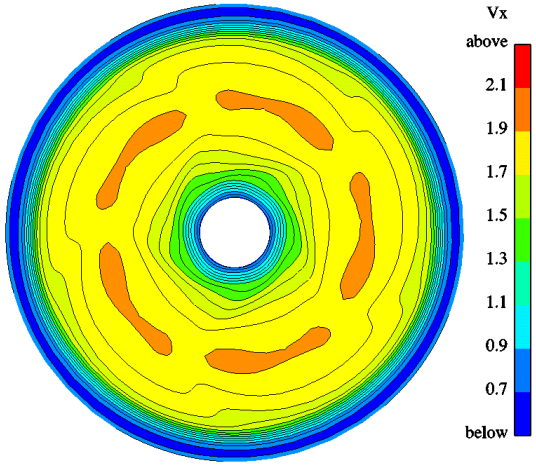

Figure 12b. Calculated velocity contours downstream of the ducted propeller (J=0.50, x/R=1.00).

Figures 12a and 12b show the velocity contours at x/R=1.00. The agreement is not so good due to numerical dissipation. It should be mentioned that a third-order upwind was used in the radial and circumferential directions and a second-order in the axial one for the calculation of the convective fluxes. Probably, the use of a third-order upwind in the axial

direction instead of a second-order discretization would have improved the results.

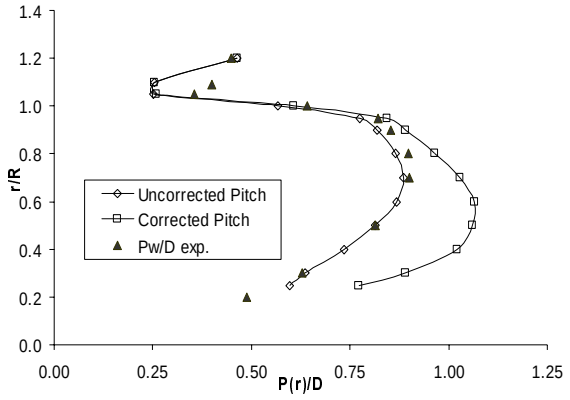

Figure 13. Comparison of calculated and experimental distribution of hydrodynamic pitch in the trailing vortex wake at x/R=0.65 for J=0.5.

Figures 8 and 9 in Kawakita (1992) show the experimental radial distribution of hydrodynamic pitch angle and of hydrodynamic pitch of the trailing vortex wake at x/R=0.65 for J=0.5. In this reference, the hydrodynamic pitch angle of the trailing vortex wake of the ducted propeller was calculated in the experiments using the averaged axial and tangential velocities v_x and v_t as

$$\beta_w = \tan^{-1}\left(\frac{v_x}{r\Omega + v_t}\right) \qquad (7)$$

It seems apparent that a small error was made when the above formula was applied: the circumferential mean tangential velocity was introduced in the formula with a positive sign instead of the correct negative one. The error resulted in a low pitch and low pitch angle that is not easy to notice. If we calculate the hydrodynamic pitch for the computational results in the same way, i.e. giving a positive sign to the v_t, the curve labeled "uncorrected pitch" in Figure 13 is obtained, which can be directly compared to Figure 9 in Kawakita (1992). The experimental data from this reference have been also included in Figure 13. The agreement is very good. On the other hand, the computed hydrodynamic pitch with the correct negative sign is presented also in Figure 13 with the label "corrected pitch." The same process can be repeated for the experimental results presented in Figure 8 by Kawakita (1992). It can be compared with Figure 14, where the computed hydrodynamic pitch angle has been calculated with and without the correction to the tangential velocity sign. The agreement with experiments is also very good. Only at the duct wake located at about r/R=1.05 did differences appear, i.e. the strength of the duct wake is a little stronger in the calculations.

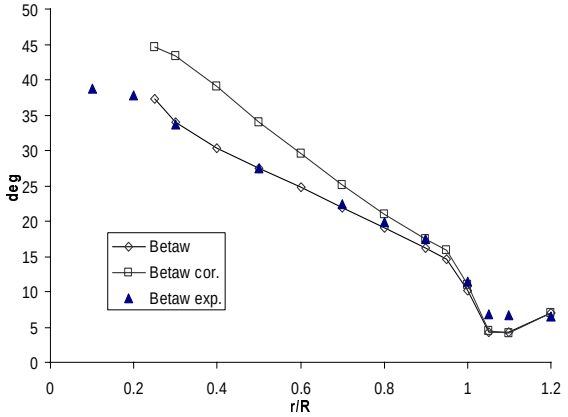

Figure 14. Comparison of calculated and experimental distribution of hydrodynamic pitch angle in the trailing vortex wake at x/R=0.65 for J=0.5.

CONCLUSIONS

The incompressible viscous flow around a Ka series propeller with NSMB nozzle 19A has been simulated by solving the RANS equations with the k-ε turbulence model. The FINFLO code was used for the calculations. The grid contained over one million cells. Good correlation with experiments is obtained in terms of force coefficients and velocity distributions in the wake at locations not far away from the duct. The thrust coefficient has been calculated without noticeable error for the design advance number; however, the torque coefficient differs from measurements by 4.5%. For other advance numbers, the differences in thrust were a little higher but reasonable, although the torque was better predicted. Important features of the flow, like the hydrodynamic pitch angle of the propeller wake and the propeller wake itself, were accurately predicted. The calculation reveals areas of low pressure at the propeller tip and duct. This

information is useful for improving a ducted propeller design from the standpoint of cavitation. The results of the computations show that RANS solvers are mature enough to provide valuable information to the designer.

ACKNOWLEDGEMENTS

This work was funded by the Technology Development Centre (TEKES) of Finland. The computing time was provided by the Centre for Scientific Computing of Finland. The authors wish to thank Dr. Jaakko Pylkkänen for the valuable help provided during this research.

REFERENCES

Abdel-Maksoud, M. and Heinke, H.-J., "Investigation of Viscous Flow Around Modern Propulsion Systems," CFD'99 International CFD Conference, 5-7 June 1999, Ulsteinvik, Norway.

Chien, K.-Y., "Predictions of Channel and Boundary Layer Flows with a Low Reynolds Number Turbulence Model," AIAA Journal, Vol. 20, No. 1, Jan 1982, pp. 33-38.

Chorin, A.J., "A numerical method for solving incompressible viscous flow problems," Journal of Computational Physics, 2:12-26, 1967.

Falcão de Campos, J.A.C., "On the Calculation of Ducted Propeller Performance in Axi-symmetric Flows," Technical Report 696, Netherlands Ship Model Basin, Wageningen, 1983.

Gibson, I.S. and Lewis, R.I., "Ducted Propeller Analysis by Surface Vorticity and Actuator Disk Theory," Proceedings of the Symposium on Ducted Propellers, the Royal Institution of Naval Architects, Teddington, England, May 1973.

Gibson, I.S., "Theoretical Studies of Tip Clearance and Radial Variation of Blade Loading on the Operation of Ducted Fans and Propellers," Journal of Mechanical Engineering Science, Vol. 6, No. 6, 1974.

Hoshino, T., "Hydrodynamic Analysis of a Ducted Propeller in Steady Flow Using a Surface Panel Method," The West-Japan Society of Naval Architects, Vol. 166, Dec. 1989, pp. 79-92.

Hughes, M.J. and Kinnas S.A., "An Analysis Method for a Ducted Propeller with Pre-Swirl Stator Blades," Proceedings of Propellers/Shafting '91 Symposium, Virginia Beach, USA, 1991.

Kawakita, C., "A Surface Panel Method for Ducted Propellers with New Wake Model Based on Velocity Measurements," Journal of the Society of Naval Architects of Japan. Vol. 172, 1992.

Kerwin, J.E., Keenan, D.P., Black, S.D., and Diggs, J.G., "A Coupled Viscous/Potential Flow Design Method for Wake-Adapted Multi-Stage, Ducted Propulsors Using Generalized Geometry," SNAME Transactions, Vol. 102, 1994, pp. 23-56.

Kerwin, J.E., Kinnas, S.A., Lee, J.T., and Shih, W.Z., "A Surface Panel Method for the Hydrodynamic Analysis of Ducted Propellers," SNAME Transactions 95, 1987 pp. 93-122.

Lehtimäki, R., Laine, S., Siikonen, T., Salminen, E., Navier-Stokes Calculations for a Complete Aircraft, 20th ICAS Congress, Sorrento, ICAS-92-4.2.1, 1996.

Lombard, C., Bardina, J., Venkatapathy, E. and Oliger, J., "Multi-Dimensional Formulation of CSCM - An Upwind Flux Difference Eigenvector Split Method for the Compressible Navier-Stockes Equations," in 6th AIAA Computational Fluid Dynamics Conference, Danvers, (Massachusetts), 1983.

Rahman, M., Rautaheimo, P., and Siikonen, T. "Numerical Study of Turbulent Heat Transfer from Confined Impinging Jets Using a Pseudo-Compressibility Method," Report 99, Helsinki University of Technology, Laboratory of Applied Thermodynamics, 1997. ASBN 951-22-3428-9.

Roe, P.L., "Approximate Riemann Solvers, Parameter Vectors, and Difference Schemes." Journal of Computational Physics, 43:357-372, 1981.

Pitkänen, H. and Siikonen, T., "Simulation of Viscous Flow in a Centrifugal Compressor. Espoo, HUT, Laboratory of Aerodynamics," Report No. B-46, 1995.

Sánchez-Caja, A., Rautaheimo, P., Salminen, E., and Siikonen, T., "Computation of the Incompressible

Viscous Flow around a Tractor Thruster Using a Sliding Mesh Technique," 7th International Conference in Numerical Ship Hydrodynamics, Nantes 1999.

Sánchez-Caja, A., "DTRC Propeller 4119 Calculations at VTT," VTT Report VALB304. Presented at 22nd ITTC Propulsion Committee Propeller RANS/Panel Method Workshop, Grenoble, April 5-6, 1998.

Siikonen, T., "An Application of Roe´s Flux-Difference Splitting for k-ε Turbulence Model," International Journal for Numerical Methods in Fluids, Vol. 21, No. 11. (Espoo, HUT, Laboratory of Aerodynamics, Report No. A-15.), 1994.

Siikonen, T. and Pan, H.-C.,1992, "An Application of Roe´s Method for the Simulation of Viscous Flow in Turbomachinery," First European Computational Fluid Dynamics Conference, Brussels, 7-11 Sep 1992.

Siikonen, T., Hoffren, J., and Laine, S., "A Multigrid LU Factorisation Scheme for the Thin-Layer Navier-Stockes Equations," Proceedings of the 17th ICAS Congress, pp. 2023-2034, Stockholm, Sept. 1990. ICAS Paper 90-6.10.3.